Satellite SAR interferometric techniques in support to emergency mapping

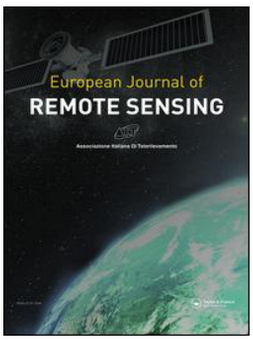

European Journal of Remote Sensing

ISSN: (Print) 2279-7254 (Online) Journal homepage: https://www.tandfonline.com/loi/tejr20

Satellite SAR interferometric techniques in support to emergency mapping

Magdalena Vassileva, Fabio Giulio Tonolo, Paolo Riccardi, Daniele Lecci, Piero Boccardo & Giuliana Chiesa

To cite this article: Magdalena Vassileva, Fabio Giulio Tonolo, Paolo Riccardi, Daniele Lecci, Piero Boccardo & Giuliana Chiesa (2017) Satellite SAR interferometric techniques in support to emergency mapping, European Journal of Remote Sensing, 50:1, 464-477, DOI: 10.1080/22797254.2017.1360155

To link to this article: https://doi.org/10.1080/22797254.2017.1360155

Published online: 09 Aug 2017.

EUROPEAN JOURNAL OF REMOTE SENSING, 2017
VOL. 50, NO. 1, 464–477
https://doi.org/10.1080/22797254.2017.1360155

Taylor & Francis
Taylor & Francis Group

Satellite SAR interferometric techniques in support to emergency mapping

Magdalena Vassileva[a], Fabio Giulio Tonolo[a], Paolo Riccardi[b], Daniele Lecci[b], Piero Boccardo[c] and Giuliana Chiesa[d]

[a]ITHACA, Torino, Italy; [b]Sarmap, Purasca, Switzerland; [c]Politecnico di Torino, Torino, Italy; [d]Geoworks, Gravere, Italy

ABSTRACT

This paper investigates the potential of Synthetic Aperture Radar (SAR) interferometry in the field of emergency mapping, assessing its suitability for both rapid mapping, aimed at supporting the immediate response phase after a disastrous event, and risk mapping, addressing risk prevention and mitigation activities. The conventional Differential Interferometric SAR technique (DInSAR) and the two currently available multi-temporal interferometric approaches, i.e. Permanent Scatterers (PS) and Small BAseline Subset (SBAS), have been evaluated focusing on the main emergency mapping requirements, namely crisis information product types, availability of optimal input data, requirements in terms of auxiliary data, processing time and expected accuracy. The aforementioned investigations have been carried out exploiting the European Space Agency (ESA) C-band Sentinel-1 mission, characterized by a free, full and open data policy. Therefore, this paper will not assess different SAR sensors and their different technical specifications, e.g. wavelength and space resolution. Representative results are presented and discussed with the aim to describe the possible interferometric product types in specific emergency mapping scenarios.

ARTICLE HISTORY
Received 1 March 2017
Revised 24 July 2017
Accepted 24 July 2017

KEYWORDS
Natural hazards; DInSAR; Permanent Scatterers (PS); SBAS; crisis information

Introduction

Emergency Mapping can be defined as the "creation of maps, geo-information products and spatial analyses dedicated to providing situational awareness emergency management and immediate crisis information for response by means of extraction of reference (pre-event) and crisis (post-event) geographic information/data from satellite or aerial imagery" (IWG-SEM, 2014). Satellite Earth Observation (EO) supports a wide range of disaster types and all phases of Disaster Risk Management (DRM), i.e. prevention and mitigation, preparedness, response and recovery, since it enables the acquisition of geospatial data over large areas with limited or no accessibility. Satellite-based emergency mapping has been increasingly used for the global rapid assessment of disaster situations and risk reduction in the last 15 years (Voigt et al., 2016). Different types of remote sensors, platforms and techniques are available: the choice is mainly based on the event details and the end-user requirements, e.g. the type of disaster to be mapped, the approximate extent of the affected areas, the required level of detail of the analysis and the need for monitoring the event (Boccardo & Giulio-Tonolo, 2014).

As far as the sensor type is concerned, Synthetic Aperture Radar (SAR) sensors, characterized by the so-called "all-weather" and "all-day" operational capabilities, represent a powerful tool also for emergency mapping: they increase the monitoring frequency exploiting satellite passes during both local morning and evening and they provide geospatial information in almost any cloud-cover condition (although some particular meteorological situation, such as the presence of thick rain cells, may interfere with the backscattered signal). SAR interferometry (InSAR) (Rosen et al., 2000) is a particular technique that can derive the terrain elevation model from two geometrically compatible SAR images, while with differential interferometry (DInSAR) (Gabriel, Goldstein, & Zebker, 1989), it is possible to extract the elevation data and detect possible surface movements. The coherence image generated during the interferometric process provides information about the interferometric quality; however, it can also be used to indirectly extract thematic information relevant to ground feature properties and their temporal changes otherwise not visible only from the amplitude information. In the past decades, the interest of the scientific community focused on multi-temporal analysis in parallel to technological breakthroughs, which made it possible to process and manage huge volumes of data, i.e. big data. In this context, two main multi-temporal stacking interferometric approaches were developed: Permanent Scatterers (PS) (Ferretti, Prati, & Rocca, 2000, 2001; Hooper, Zebker, Segall, & Kampes, 2004) and Small BAseline Subset (SBAS) (Berardino, Fornaro, Lanari, & Sansosti, 2002). SAR interferometry is a powerful satellite technique for the assessment of

CONTACT Magdalena Vassileva magdalena.vassileva@siti.polito.it ITHACA, via P.C. Boggio 61, Torino 10138, Italy

geological hazards and may contribute to emergency mapping by providing unique geospatial information.

This paper investigates the potential of the currently available interferometric algorithms for the extraction of crisis information useful for emergency management activities, with a focus on the type of crisis information that can be exploited in this domain. First, the interferometric techniques are briefly explained focusing mainly on topics relevant to emergency mapping applications. Second, the described techniques are analyzed and discussed, with the main aim to assess the usefulness of the information extracted by means of an interferometric approach and the fulfillment of the emergency mapping requirements. The analysis is summarized according to five main parameters that have been identified as relevant for emergency mapping: type of crisis information that can be extracted, availability of optimal input data, requirement in terms of auxiliary data, processing time and expected accuracy. The final section presents and discusses several operational tests (referencing actual case studies when possible), performed exploiting the Commercial off-the-shelf (COTS) software ENvironment for Visualizing Images (ENVI) SARscape module and using the Copernicus Sentinel-1 SAR images and the 90 m Digital Elevation Model (DEM) provided by the Shuttle Radar Topography Mission (SRTM) as the input dataset.

SAR interferometric techniques

SAR imagery (Single Look Complex product type) is an array of complex values composed of the amplitude information and the phase shift of the backscattered signal. The phase shift itself does not provide any useful information. However, the phase difference, or interferogram, between two SAR acquisitions with compatible geometries contains information about surface topography and possible ground displacements in the Line of Sight (LOS) direction. Many other factors contribute to the phase difference, but they do not provide useful information for emergency mapping and thus their effects should be removed or at least reduced, i.e. geometric decorrelation, temporal decorrelation, imprecise orbit information, atmospheric disturbance and sensor noise. Specifically, DInSAR is the method applied to obtain surface deformations by subtracting the terrain elevation.

The interferogram values range between $\pm\pi$ and, therefore, it is displayed as a series of fringes. The 2π change in the interferometric phase – referred to as interferometric ambiguity – corresponds to a certain amount of height change or displacement that can be measured. This parameter determines the phase sensitivity to topographic variation or surface displacement, and thus the minimum topographic variation or movement detectable by the SAR interferometric system. The interferometric topographic ambiguity depends on: i. the normal baseline (Bn), i.e. the orthogonal component of the distance between the positions of the two sensors; ii. the signal wavelength (λ); iii. the sensor–target distance (R) and iv. the incidence angle (θ):

$$(\Delta \boldsymbol{h}=(\boldsymbol{\lambda} \times \boldsymbol{R} \times \sin\boldsymbol{\theta})/(2 \times \mathrm{Bn})) \quad (1)$$

The interferometric displacement ambiguity is equal to $\lambda/2$ and thus the displacement along the sensor–target LOS can be detected up to the centimeter level. Generally, the topographic sensitivity increases along with the length of the normal baseline, without exceeding the so-called critical value for which the phase becomes inconsistent (see Figure 1 (a)). On the other hand, the displacement sensitivity decreases along with the length of the normal baseline and the ideal condition would be to reach null B_n values (see Figure 1(b)).

In order to obtain physical information, i.e. elevation or surface movement, the interferogram has to

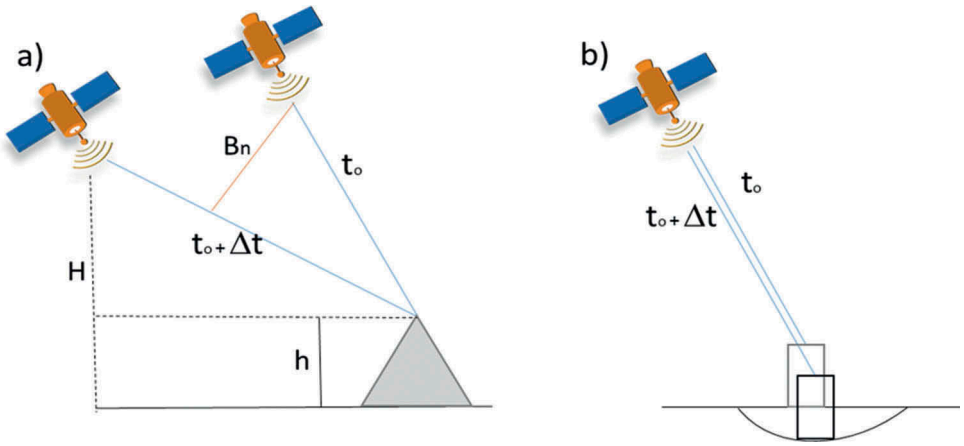

Figure 1. Repeat-pass SAR acquisition (t_0 refers to the first acquisition time and t_0+?t refers to the second acquisition time). Acquisition geometric configuration suitable a) for topographic detection; H is the orbital altitude and h is the elevation of the target; b) for surface deformation.

be unwrapped. This step is performed by complex algorithms that transform the ambiguous 2π values in absolute values with respect to one or more reference points.

The accuracy of the physical values depends on, in addition to the interferometric ambiguity, several parameters hardly computable a priori: decorrelation, both geometric and temporal, atmospheric effects, noise, additional data accuracy, and processing constraints. Geometric decorrelation is induced by the presence of multiple comparable scatterers within a single ground cell that vary their reflectivity response as the acquisition geometry changes. This effect is present, for instance, in vegetated areas. Temporal decorrelation is triggered by seasonal changes or changes in land use; therefore, short time differences are preferred in order to reduce temporal decorrelations. The coherence estimation is a useful parameter to obtain information about the geometric and temporal decorrelation. It is a cross-correlation product derived from two co-registered complex-valued SAR images and it estimates the statistical differences between the signals in the two acquisitions.

The well-known SAR perspective distortions are another relevant factor for the determination of the final data accuracy. Layover and shadowing alter the amplitude and phase information and consequently no useful data can be extracted over those zones. Areas with no data may be reduced by combining ascending and descending acquisition geometries (Crosetto, 2002). Layover and shadow masks may be generated a priori in order to understand whether the area of interest is affected by distortions.

Two different multi-temporal stacking interferometric approaches were developed in the past decades: PS and SBAS. These advanced techniques are applied to detect the temporal evolution of surface deformations and to overcome some of the limitations encountered in simple differential interferometry: removal of atmospheric effects and baseline decorrelation phenomena, high coherence, and robustness with respect to possible errors of the DEM (Berardino et al., 2002; Lanari et al., 2007). Both approaches require a temporal dataset of subsequently acquired SAR images with compatible geometries. The multi-temporal approach improves interferometric performance and sensitivity, detecting up to millimeter displacement. However, the PS and SBAS approaches present essential performance differences. The PS approach is based on the identification of persistent point-wise reflectors, such as man-made structures and rocks, presenting high coherence over the whole period of observation and providing point-wise displacement estimation only for the detected stable targets. Owing to this characteristic, the PS technique exploits all the interferometric pairs, and thus, those characterized by long baselines. In fact, all interferograms are generated in relation to the same master image. The major limitation of the PS approach is given by the heterogeneity of the PS identified by the algorithm over areas with different land cover: higher density in urban areas, lower density in nonurban areas, even null in vegetated areas. On the other hand, the SBAS approach consists of the combination of images with SBAS in order to limit spatial decorrelation effects. In order to follow the displacement evolution over time, the different interferograms must be connected in time (see Figure 2). The surface displacement is then generated over distributed scatterers with homogeneous characteristics, such as short-vegetated, debris or desert areas, which exceed a certain coherence threshold (normally 0,2).

As mentioned above, SAR interferometry can measure only one dimension of the LOS surface deformation component. If the displacement happened orthogonally to the LOS direction, this component is null. Positive values correspond to a movement toward the sensor, whereas negative values correspond to a movement backward from the sensor. Phase difference is mostly sensitive to vertical displacements rather than to horizontal ones. Furthermore, there is no sensitivity to orbital direction (north–south) movements. The real direction of deformation can be detected by combining two acquisition

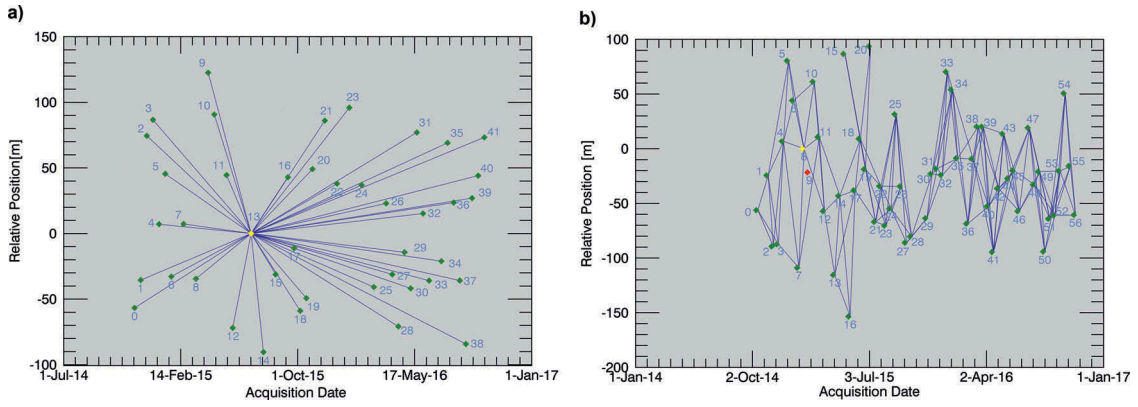

Figure 2. Example of connection Graph plotted in SARscape: A) PS; b) SBAS.

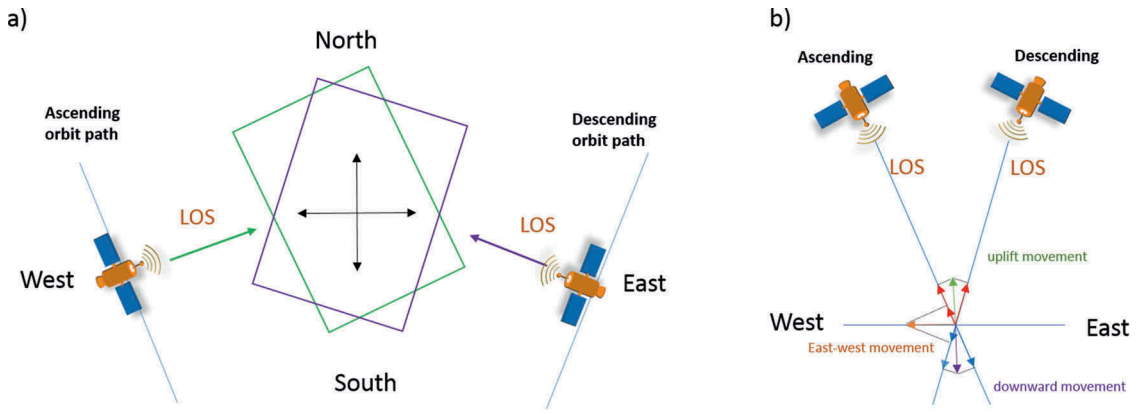

Figure 3. SAR interferometric surface deformation detection from ascending and descending orbital path: (a) image orientation; (b) LOS component (in red positive movement and in blue negative movement), vertical component (in green uplift movement and in violet downward movement) and east–west component (in orange from west to east movement).

geometries, i.e. ascending and descending (see Figure 3(a)). The surface movements identified in both geometries can be interpreted in the following way (see Figure 3(b)).

- Same signs of movement value in both geometries indicate predominantly vertical movements, positive if uplift and negative if downward
- Opposite signs of movement value in both geometries indicate that the movement is from east to west (or vice versa)

Displacement measurements are always relative to time and space: relative to time because the movement is calculated with respect to one master image acquired in a specific period and relative to space because all movements are computed with respect to a specific reference point (assumed as stable).

SAR interferometry capabilities in emergency mapping

Emergency mapping is aimed at supporting emergency management activities. Two main different emergency mapping types exist: rapid mapping, i.e. the fast provision of geospatial data required for the immediate emergency response phase, and risk monitoring mapping, i.e. the monitoring of specific parameters over time in risk-prone areas. The rapid mapping usual workflow consists of a multi-temporal analysis exploiting one pre-event and one (or more) post-event image acquired immediately after the event. According to the disaster type, two main types of crisis information can be derived: delineation of the event extent, e.g. flooded areas, landslide body and forest fires, and damage assessment, e.g. damage levels to buildings, infrastructures and agricultural fields. Different sensors (e.g. optical, microwave, hyperspectral, etc.) and approaches (e.g. indexes, visual interpretation, change detection techniques, etc.) are used in emergency mapping. SAR data exploitation is predominant for flooded area extraction (Vassileva, Nascetti, GiulioTonolo, & Boccardo, 2015), while optical imagery is exploited especially when damage assessment is requested (Antonietta, Boccardo, Giulio Tonolo, & Vassileva, 2015). Automatic and semiautomatic methods are preferred in order to speed up the processing steps and the thematic information extraction. Monitoring mapping requires continuous measurements over the area of interest in order to control the evolution of the phenomena, e.g. drought (Perez, Cámaro, Angeluccetti, Demarchi, & Boccardo, 2015).

In the last decade, emergency managers increased their interest in SAR interferometric products, especially thanks to the new high-resolution SAR missions (e.g. the next-generation TerraSAR-X Staring SpotLight Mode, with a Ground Sample Distance up to 0.25 m), advanced processing approaches and powerful software.

This paper aims at providing an overview of the potentials and limitations of the aforementioned interferometric approaches, i.e. InSAR, DInSAR, PS and SBAS, applied to emergency mapping. Five parameters have been identified and analyzed: i. crisis information product types; ii. availability of optimal input data; iii. requirement in terms of ancillary data; iv. processing time and v. expected thematic accuracy.

Crisis information product types

The conventional interferometric technique (InSAR) allows the generation of digital elevation maps, whereas differential interferometry (DInSAR) provides deformation mapping in the LOS direction. DInSAR is suitable to map large and quick surface movements, such as the ones induced by earthquakes (Zuo, Qu, Shan, Zhang, & Song, 2016) or by immediate slope failures (Casagli et al., 2016). A coherence image is also produced for each generated interferogram. The coherence combined with amplitude information is exploited in the Multi Temporal Coherence (MTC) color composite approach

to detected changes on the ground not visible from the amplitude information only. This approach is successfully applied to new lava flow detection (Boccardo, Gentile, Giulio-Tonolo, Grandoni, & Vassileva, 2015).

PS and SBAS can detect slow target movements as the ones related to rotational and translational landslides (Bianchini et al., 2015; Haghighi & Motagh, 2016), rock flows (Piacentini et al., 2015) and subsidence phenomena (Zhang, Huang, & Bi, 2014; Zhu et al., 2015). These advanced interferometric techniques are applied to generate mean deformation velocity maps and displacement time series in the LOS direction. PS provides point-wise measurements in urbanized and outcrops areas, where stable scatterers are mostly present. Therefore, no information can be provided in agricultural and natural vegetated areas. SBAS provides spatially dense deformation maps, due to the possibility to detect changes also over short-vegetated or non-vegetated areas.

Emergency management deals mostly with sudden onset events that strike and develop in a short time or are activated in particular environmental conditions, e.g. earthquakes or landslides due to intense rain. Therefore, conventional interferometric techniques are mostly suitable, in terms of thematic content, for rapid mapping purposes since they can detect sudden surface deformations (but also the timeliness of the availability of such information to the end-users should be considered when evaluating them as fit-for-purpose for rapid mapping). Elevation models generated through the InSAR technique can provide more accurate topographic information useful in flood analysis (Mason et al., 2016), and for the geometric correction of optical imagery. PS and SBAS temporal analyses are mostly appropriate for long evolution phenomena and thus for monitoring mapping. The main considerations are summarized in Table 1, while detailed examinations of the factors follow right after.

Availability of optimal input data

SAR interferometry for DEM generation requires one SAR image pair, characterized by suitable geometries (same sensor, same orbit and same path). The pair should have a normal baseline as long as possible (but without exceeding the critical baseline) in order to introduce the smallest ambiguity between the fringes and should be characterized by a short time difference in order to reduce temporal decorellations. To compensate for the lack of information over parts of the analyzed area due to radar distortion phenomena, at least two different geometries should be processed and integrated.

DInSAR requires a pair of SAR images, one before and one after the event, with a baseline as short as possible in order to reduce the elevation residual phase. A third SAR image or a DEM is required to perform the elevation subtraction. The real surface deformation vector may be estimated by combining the two geometries (i.e. ascending and descending). PS and SBAS require large time dataset of SAR scenes (at least 20 images). The images have to be acquired from the same sensor, have the same acquisition geometries and be characterized by good temporal sequence continuity.

All the aforementioned requirements can be fulfilled due to the availability of different SAR missions currently operational and providing a large amount of data (see Figure 4). The frequency of image availability over a certain area of interest depends on the satellite revisiting time and the sensor operational mode, i.e. continuous or on-demand acquisitions. Some commercial missions, such as the Italian Cosmo-SkyMed (2016), acquire regularly over some areas (at least one acquisition per month is guaranteed over the Italian territory), and only on demand over other areas. The currently operational Sentinel-1 mission acquires continuously worldwide with a 6-day revisiting time after the launch of its second satellite Sentinel-1B in April 2016 (the Sentinel-1B image public availability started on 26 September 2016). All the operational missions' acquisition can be replanned in case of emergency in order to cover priority affected areas and to provide the required dataset in the shortest time possible, i.e. near real time.

Table 1. Summary table of the interferometric approaches analyzed with respect to five parameters: processing time values are related to Sentinel-1 image processing tests, entire IW scene in the case of DInSAR and InSAR processing, and 25–30 images of about 100 km^2 extent in the case of PS and SBAS processing.

	InSAR	DInSAR	SBAS/PS
Product types	DEM	Deformation map	Mean velocity deformation map, time evolution deformation stack
Availability of optimal images in input	Pair of SAR images with suitable geometries, short time baseline, normal baseline as long as possible	Pair of SAR images with suitable geometries, short time baseline, normal baseline as short as possible	Temporal dataset of at least 20 SAR images with suitable geometries and with a good temporal sequence continuity
Requirement of additional data	DEM, precise orbits	DEM, precise orbits	DEM, precise orbits
Processing Time	5–6 h	5–6 h	12 h, with computer clustering the processing time is reduced to 4–5 h
Expected theoretical accuracy of the result	up to meter level	up to centimeter level	up to millimeter level

No ground data were used to validate the accuracy, and thus the table reports the expected theoretical accuracy values.

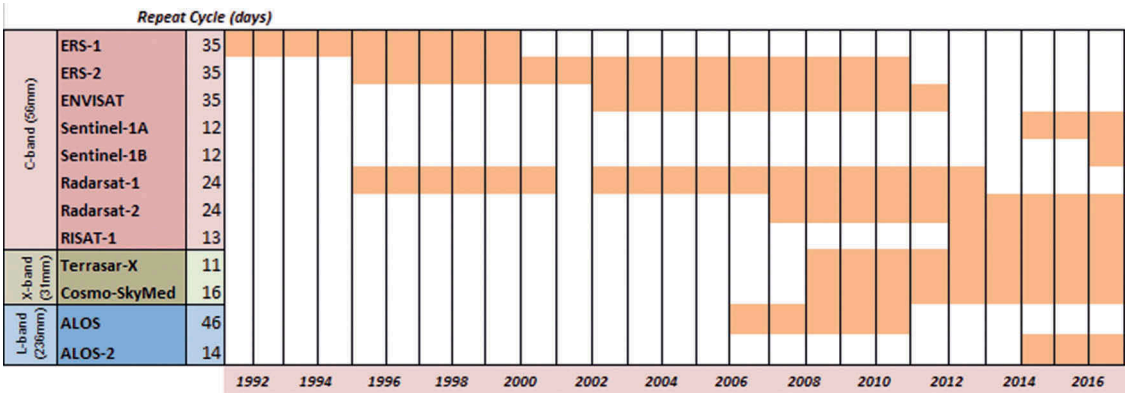

Figure 4. Main satellite SAR missions.

Requirement of additional data

To correctly process SAR data, precise orbit information may be needed. SAR images acquired by Cosmo-SkyMed and Terrasar-X satellites are disseminated directly with the precise orbits information, whereas SAR images acquired with ERS-1, ERS-2, ENVISAT ASAR, Radarsat and Sentinel-1 require an external file. In particular for Sentinel-1 acquisitions, the estimated orbit data are delivered after a few hours from the data acquisition, while the precise information is delivered only after almost 2 weeks from the acquisition. However, possible errors due to imprecise orbits can be modeled and removed during the post-processing interferometric phase.

An external DEM is required for displacement maps, velocity maps and elevation model generation. For deformation detection, a high-resolution elevation model is required in order to remove the topographic contribution from the interferogram. In case of DEM generation, a low-resolution elevation model is sufficient as the input dataset. For example, SRTM with 1-arch sec (~30 m at the equator) pixel spacing and 16 m estimated height accuracy, with a global coverage with latitudes in the range from 56° S to 60° N, is a good starting point in case more accurate elevation models are not available.

In the interferometric refinement and unwrapping phases, Ground Control Points should be properly selected over the image in stable and flat areas, avoiding areas subject to movements or with high elevation discontinuities. Furthermore, in order to correct the aforementioned orbital errors, the GCPs should be homogeneously distributed over the whole image.

Processing time

The interferometric processing time depends on image resolution, image size, number of images to be processed, number of interferograms to be generated and hardware technical features.

The operational tests that will be described and discussed in this paper were carried out with ENVI SARscape COTS software installed on a computer with the following technical features: Windows 10 Pro, Intel Xeon E5-2670 2.6GHz, 2 CPUs, 8 cores per CPI, 64GB RAM.

The map displacement or DEM generation processing steps in SARscap are: 1. Interferogram Generation; 2. Adaptive Filter and Coherence Generation; 3. Phase Unwrapping; 4. Refinement and Re-flattening; 5. Phase conversion and Geocoding. The interferogram generation and unwrapping processing are the most time-consuming steps. One entire Sentinel-1 scene (20 x 20 m^2 pixel size) requires about 1.5 h to produce an interferogram image. The final product is obtained in almost 5–6 h.

PS and SBAS techniques are highly time-consuming because of the high number of images required in the operation and the high number of interferograms generated. The SAR data processing time (starting from the downloading of the image until the final processing step) proportionally increases with the number of images to be processed. The following steps are performed in the SARscape PS processing chain: 1. Connection Graph; 2. Interferometric Process; 3. First Inversion Step; 4. Second Inversion Step; 5. Geocoding. The SARscape SBAS processing workflow is composed as follows: 1. Connection Graph; 2. Interferometric Process; 3. Refinement and Re-Flattening; 4. First Inversion; 5. Second Inversion Step; 6. Geocoding. The most time-consuming steps are the interferogram process and the first inversion step (see Figure 5). For very large datasets (50 and more images), these steps may require as long as 1 week.

To speed up the most time-consuming steps, Sarmap group developed a SARscape computer clustering performance. The cluster architecture comprises one client machine, which spreads the serial traces between many nodes connected to it. In such a way, image co-registration, interferogram formation, unwrapping (in the case of SBAS) and first inversion are processed in parallel. Thereafter, the client machine recalls the results,

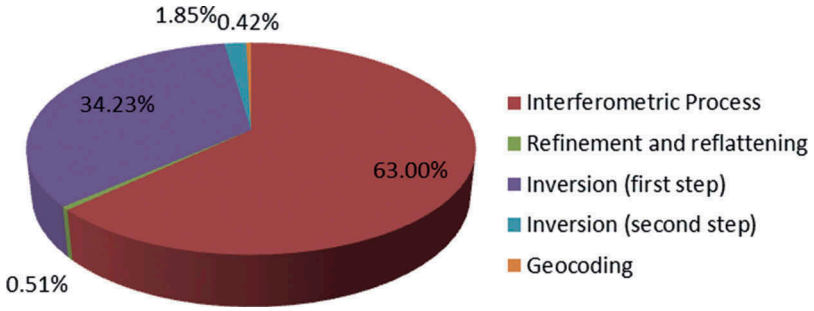

Figure 5. SBAS processing time on a single machine. The "Connection graph" time is negligible and therefore it is not shown in the chart (© 2016 sarmap).

assembles the separate parts and performs the non-serial steps. A specific performance test has been conducted by Sarmap: the SBAS approach using a stack of 25 COSMO-SkyMed stripmap images, 30 km × 40 km extent in urban areas (Rome, Italy), with 3 × 3 multilooking and generating 150 interferograms. The trend in Figure 6 shows that the whole SBAS time processing decreases from 10 days to almost 40 h using eight nodes. The trend converges to a minimum threshold, considering that network connectivity and disk access times highly impact the cluster performance.

Accuracy of the result

In principle, SAR interferometry has the potential to detect ground surface movement with displacement accuracies up to the millimeter level and surface elevation accuracies to the meter level. Furthermore, last-generation SAR missions, such as the German TerraSAR-X and the Italian Cosmo-SKyMed, allow images to reach spatial resolution up to 25 cm and 1 m, respectively. However, several factors, such as geometric decorrelation, temporal decorrelation, normal baseline, additional data accuracy, radar distortions and processing errors (during unwrapping), can affect both surface deformation and topographic measurements. The surface deformation accuracy is also conditioned by the movement aspect and inclination: SAR interferometry is mostly sensitive to vertical and west–east movements, while it has no sensitivity to north–south movements. The developing of advanced multi-temporal SAR interferometric techniques and the availability of new high-resolution SAR sensors with a short revisiting time eliminate the effect of several limiting factors affecting DInSAR, thereby improving the surface deformation accuracy and reaching almost the theoretical level (Prati, Ferretti, & Perissin, 2010). However, in PS and SBAS advanced approaches some errors persist, especially in relation to velocity modeling, unsuitable reference points, residual DEM and unwrapping processing (performed in the SBAS approach). The deformation accuracy may be increased by using larger and denser SAR image datasets and more accurate elevation data. To validate the SAR interferometric results, in situ data, such as GPS and leveling measures, are requested (Colesanti, Ferretti, Prati, & Rocca, 2003; Tofani, Raspini, Catani, & Casagli, 2013).

Example of SAR-based crisis information

The scope of this section is to present clear examples of SAR interferometric products and to describe the geospatial information that can be retrieved and its possible

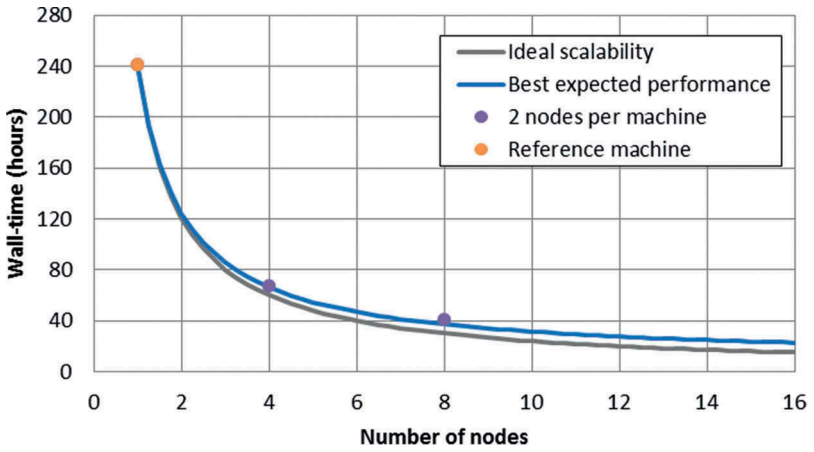

Figure 6. SBAS process time versus the number of cluster nodes: The processing time (25 COSMO-SkyMed stripmap images, 30 km × 40 km extent, 3 × 3 multilooking, generating 150 interferograms) decreases from 10 days to almost 40 h in case of eight nodes (© 2016 sarmap).

application in the emergency mapping domain, referencing actual case studies when possible. In particular, the focus is on four disaster types: earthquake, volcano eruption, subsidence and landslide. All tests have been performed with COTS software (ENVI/SARscape) and exploiting the free and open access European Space Agency (ESA) Copernicus Sentinel-1 SAR images and the open SRTM 90 m DEM. Sentinel-1 mission is characterized by stringent orbit control, which ensures a small baseline between the acquisitions. This characteristic makes Sentinel-1 data perfectly suitable for detecting surface movements; however, they are not optimal for DEM extraction.

DInSAR investigation to better understand earthquake faulting (Central Italy – August 2016)

Two pairs of multi-temporal Sentinel-1 images (Copernicus Sentinel data [2016]) acquired before and after the event (one pair acquired during ascending path – Figure 7(b) – and the other acquired during descending path – Figure 7(a)) were processed. The images were selected with the criteria of short time baselines in order to reduce possible temporal decorrelations. The short normal baseline, required for deformation detection, is almost always guaranteed from Sentinel-1 acquisition, due to the Earth-fixed orbital tube of a diameter of 100 m during normal operation.

In both geometries, thick concentric fringes are detected over the same zones affected by earth shakes. Each fringe corresponds to half wavelength (i.e. 2.9 cm for the C-band). By counting the fringes starting from the further to the central, the maximum surface deformation can be estimated. It is possible to count seven fringes, which respond to 20 cm of downward maximum deformation.

The deformation maps (see Figure 8) are obtained after the unwrapping process and the final phase to displacement conversion. The values are expressed in meters. The maps show the absolute displacement LOS component in the two geometries. The same zone emerges as negative in both geometries, i.e. surface deformation is away from the sensors, and thus the major movement is downward.

SAR interferometry applied to earthquakes allows scientists to understand how deformation occurs over a regional scale, improve earthquake models and investigate the future seismic hazard (Harris, 1998; Jónsson, Zebker, Segall, & Amelung, 2002; Marquardt, 1963; Mogi, 1958). In rapid mapping applications, interferogram and deformation maps could help identify (through ad hoc modeling) the most affected areas in order to prioritize the damage assessment over these regions. Examples of interferogram earthquake mapping have been produced by the Geo-hazard team within the Beyond project (Central Italy earthquakes, 10/2016, 2016).

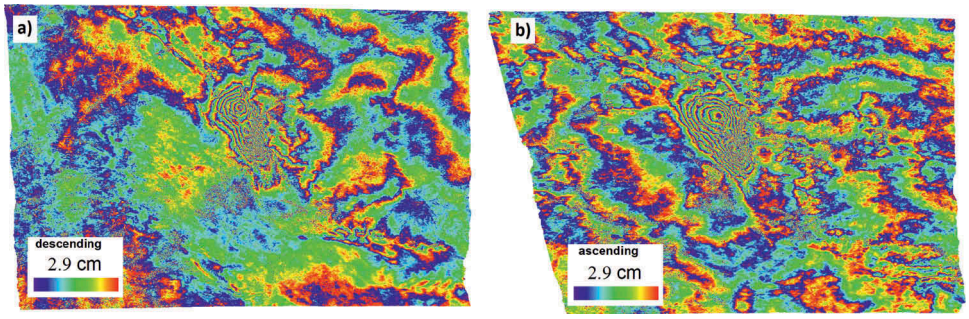

Figure 7. Interferograms of Central Italy detect fringe anomalies due to the earthquake of August 2016. The results derive from: (a) descending Sentinel-1 pair acquired on 21 and 27 August; (b) ascending Sentinel-1 pair acquired on 22 and 28 August.

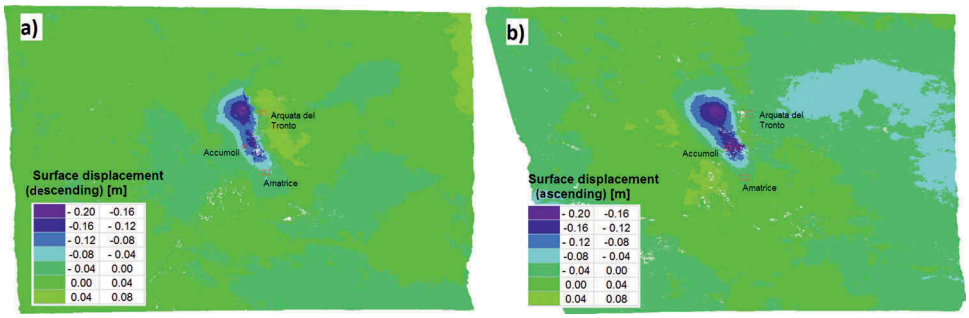

Figure 8. Deformation maps of Central Italy show the main deformation zones after the earthquake of August 2016; the results derive from: (a) descending Sentinel-1 pair acquired on 21 and 27 August; (b) ascending Sentinel-1 pair acquired on 22 and 28 August.

Monitoring of magma activity in volcanoes (Fogo, Cape Verde – 2014)

The SAR interferometry was applied to a pair of ascending Sentinel-1scenes (Copernicus Sentinel data [2014]), one before and one after the volcano eruption, and characterized by a 1-month temporal baseline. The interferometric image (Figure 9, left) shows a concentration of fringes over the volcanic sides related to magma activity, where surface deformations are also detected (Figure 9, right).

Volcano application of interferometric techniques allows scientists to monitor magma activities by analyzing surface deformation patterns and predict possible eruptions.

Lava flow detection using multi-temporal coherence analysis (Fogo, Cape Verde – 2014)

The aforementioned Sentinel-1 image (Copernicus Sentinel data [2014]) pair was processed to generate the coherence image. The Multi-Temporal Coherence product is generated combining into a single RGB color composite pre-event amplitude image (Red channel), post-event amplitude image (Green channel) and SAR interferometric coherence (Blue channel). The areas covered by recent lava flow are characterized by very low coherence due to the occurred ground changes as well as medium values in either pre- or post-event amplitude images, because of the roughness of the lava surface compared with the terrain surface conditions before the lava flow. Those areas are characterized by reddish and greenish tones (see the red box in Figure 10) (Boccardo et al., 2015).

The coherence information used jointly with the amplitude master and slave data can detect surface changes related mostly to roughness changes instead of real land-cover changes (e.g. vegetated to agricultural). This method proved to be very useful for rapid assessment during volcano eruption and in fact it was applied during the rapid mapping activation of the Copernicus Emergency Management Service for the volcanic eruption at Fogo Island (EMSR111, 2014).

Subsidence monitoring with SBAS (Mexico City, Mexico)

A set of 27 descending Sentinel-1 images (Copernicus Sentinel data [2014, 2015]), acquired in the period from 15 October 2014 to 1 November 2015, was used to perform SBAS processing. From the mean velocity displacement map shown in Figure 11 (values are expressed in mm/year), the subsidence area is well visible (bluish areas).

SBAS multi-temporal deformation analyses detect distributed deformations with annual millimeter-level trends. Therefore, they are appropriate for long-term monitoring emergency mapping rather than for rapid mapping.

Subsidence monitoring with PS (Mexico City, Mexico)

The same previous set of 27 descending Sentinel-1 images (Copernicus Sentinel data [2014, 2015]), acquired in the period from 15 October 2014 to 1 November 2015, was used to perform PS processing over a small area over Mexico City. The mean velocity displacement map is expressed in mm/year (see Figure 12). The result was compared to the SBAS mean displacement velocity.

The deformation time plot (Figure 13) computed for the same target shows a perfect agreement between the PS and SBAS techniques.

PS multi-temporal deformation analyses detect point-wise deformations with annual millimeter-

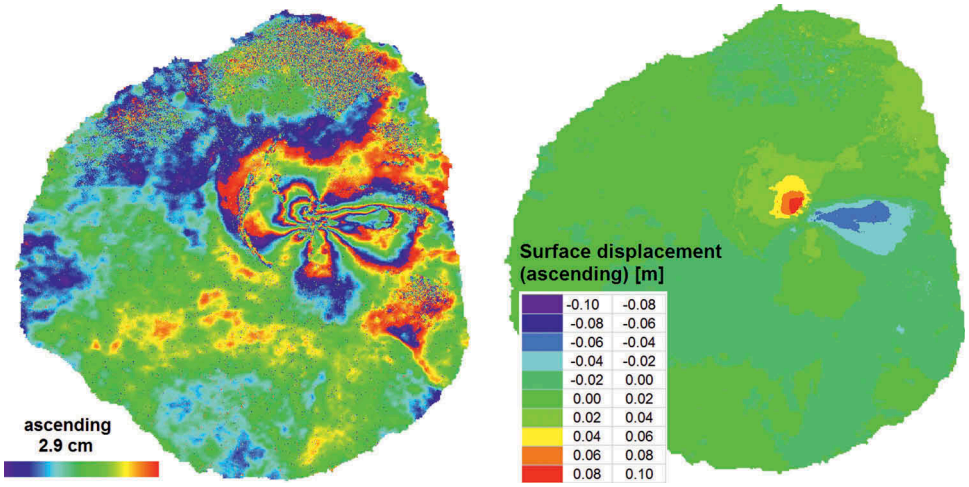

Figure 9. Interferogram (on the left) and deformation map (on the right) of Fogo Island (Capeo Verde) detect surface deformations due to the volcanic activities that occurred in November 2014; the results are derived from ascending Sentinel-1 pair acquired on 3 and 27 November.

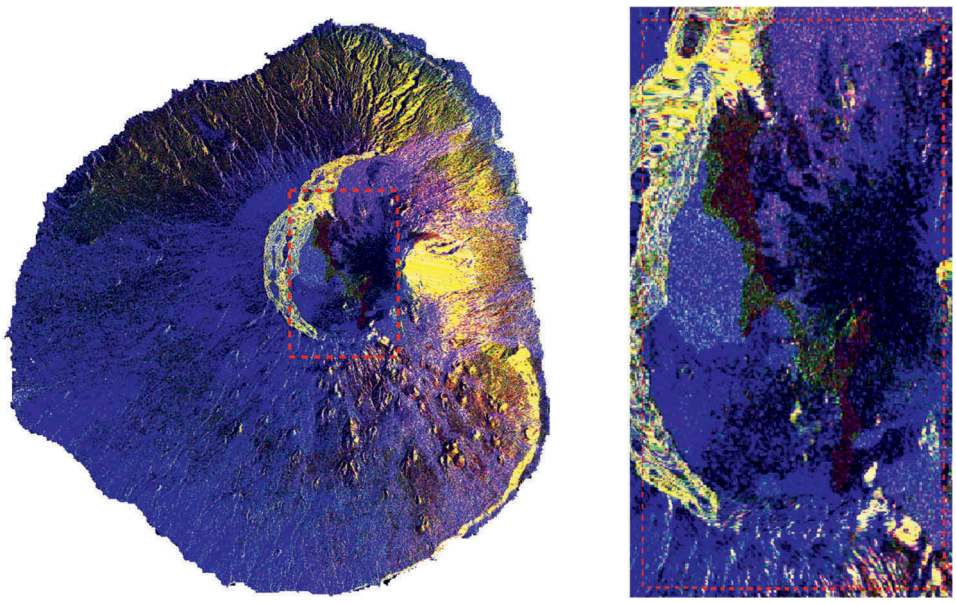

Figure 10. Multi-Temporal Coherence of Fogo Island detects new lava flow due to the volcanic eruption of November 2014. MTC is based on the combination of the pre- and post-event SAR amplitude and coherence data. The following information is associated with the three color canals: master amplitude to red canal, slave amplitude to green canal and coherence to blue canal. In the red box the reddish and greenish tones correspond to the new lava flow zones. The results are derived from ascending Sentinel-1 pair acquired on 3 and 27 November.

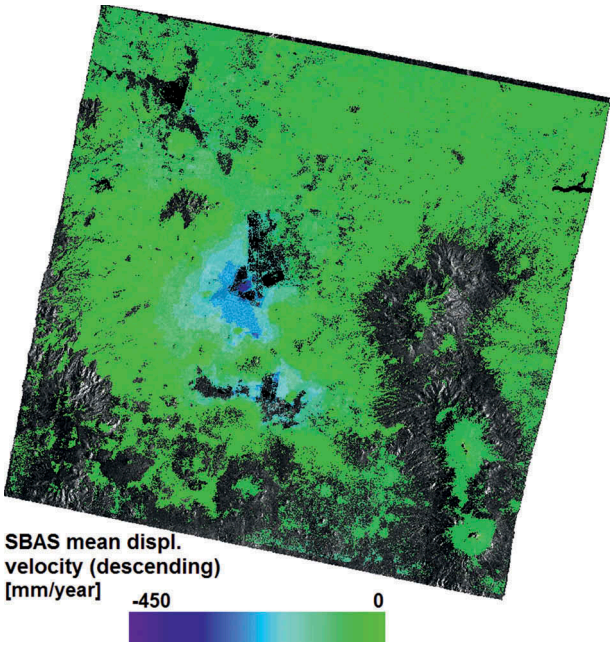

Figure 11. Mean velocity deformation map of Mexico City derived from SBAS processing and exploiting descending Sentinel-1 dataset of 28 images acquired during the period 15 November 2014 and 1 November 2015; the map detects intense subsidence phenomena over the urban area.

level trends. Therefore, they are appropriate for urban areas' long-term monitoring.

Landslide monitoring in low vegetated and urbanized area (Oulx, Italy)

Two Sentinel-1 image datasets, one ascending and one descending, were processed using the PS approach. The ascending dataset was acquired in the period from 16 November 2014 to 30 September 2016, while the descending dataset was acquired between 10 October 2014 and 23 October 2016 (Copernicus Sentinel data [2014, 2015 and 2016]). The mean LOS displacement velocity obtained from the two geometries (ascending in Figure 14(a), descending in Figure 14(b)) is comparable to downward movements, prevalently in the south–west to north–east direction.

The deformation time plot (Figure 15) of the ascending and descending acquisition geometries shows the relative movement trend in the LOS direction. In order to obtain the real direction of the movement, the two results should be merged.

PS multi-temporal interferometry is suitable to monitor in time landslide extension and kinematics in areas covered with persistent scatterers, i.e. building, infrastructures and rocks.

The Italian Piemonte Regional Environmental Protection Agency published PS analyses of a large part of the regional territory on a public Geoportal (ARPA Piemonte 2016). These analyses were carried out within the trans-boundary project RiskNat.

Conclusions

In this paper, the space-borne SAR interferometric capabilities have been presented, discussing the potential applications in the emergency mapping domain. For this purpose, ESA's C-band Sentinenel-1 acquisitions have been exploited for the operational tests focused on four disaster types: earthquake, volcano eruption, subsidence and landslide. The

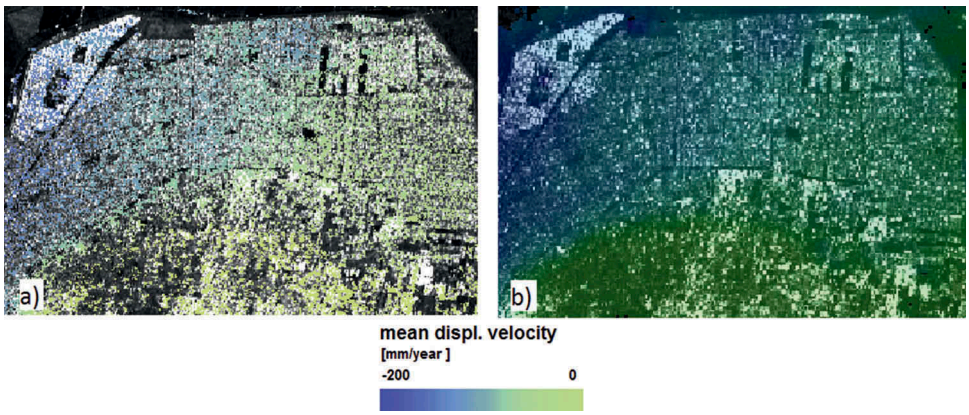

Figure 12. PS and SBAS mean displacement velocity of East Mexico City derived from the same descending Sentinel-1 dataset of 28 images acquired in the period from 15 November 2014 to 1 November 2015: (a) PS interferometric processing; (b) SBAS interferometric processing. Equal histogram interval is set in visualization.

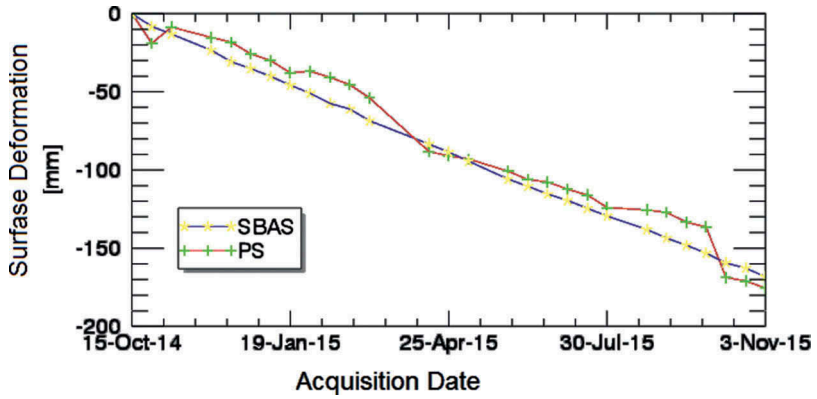

Figure 13. The plot shows the displacement time series of a specific unstable target over East Mexico City detected from PS and SBAS processing and exploiting the same descending Sentinel-1 dataset of 28 images acquired in the period between 15 November 2014 and 1 November 2015. The comparison demonstrates good consistency between the PS and SBAS results.

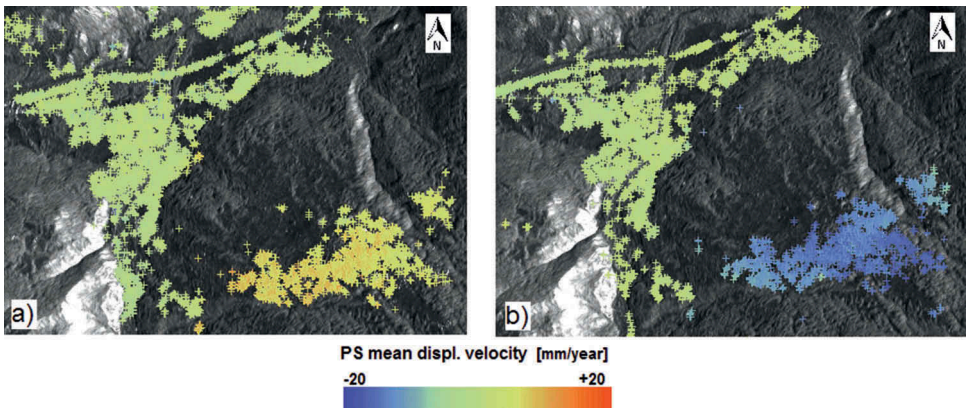

Figure 14. PS ascending and descending mean displacement velocity maps of Oulx (Italy) show surface movement over landslide-prone areas. The results were obtained from: (a) ascending Sentinel-1 dataset of 41 images acquired between 6 November 2014 and 30 September 2016; (b) descending Sentinel-1 dataset of 56 images acquired between 10 October 2014 and 23 October 2016.

processing steps have been carried out with the COTS software ENVI/SARscape.

The interferogram image and the deformation map produced through DInSAR have proven to be able to detect large-scale and sudden surface movements, such as the ones caused by earthquakes. Nevertheless, it needs to be remarked that DInSAR applied to slope failure detection may not produce useful information in case of smaller-scale landslides, when using low-resolution Sentinel-1 images coupled with a low vertical accuracy DEM or when analyzing vegetated areas.

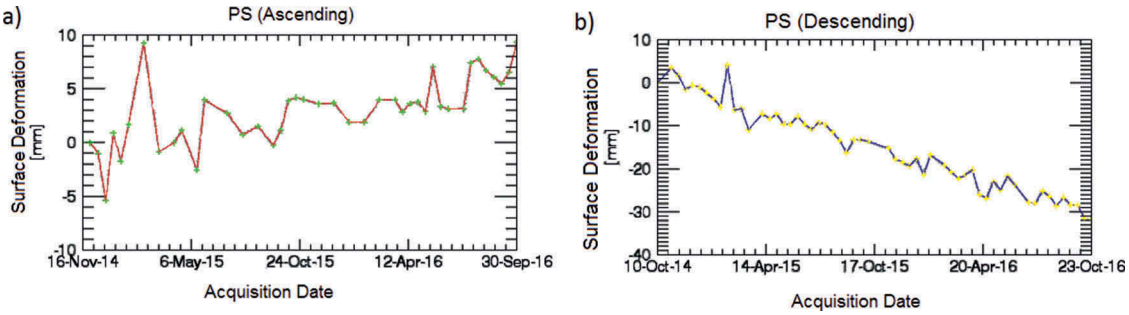

Figure 15. Displacement time series plot over a specific unstable target over the landslide-prone areas in Oulx (Italy): (a) PS processing ascending Sentinel-1 dataset of 41 images acquired between 6 November 2014 and 30 September 2016; (b) PS processing descending Sentinel-1 dataset of 56 images acquired between 10 October 2014 and 23 October 2016.

SAR coherence-based products are useful tools in case of surface deformations affecting the radar backscattering (both phase and amplitude) such as the ones induced by a new lava flow.

Multi-temporal interferometric techniques, such as PS and SBAS, are able to monitor the temporal evolution of slow movements, but they require as input data large temporal datasets of SAR imagery characterized by suitable geometries and uniform distribution over time. These advanced techniques provide more reliable deformation values and may achieve up to millimeter-level deformation accuracy.

Considering that ground information is most often not available in an emergency mapping context, both SBAS and PS should be applied to validate the results and avoid false detection, therefore considering as reliable only the surface deformations confirmed by both techniques. Particular deformation geometries, as in the case of unstable slopes and active faults, require processing both ascending and descending orbit data.

The final results of the aforementioned interferometric approaches are highly affected, in all cases, by the ancillary DEM vertical accuracy, the SAR image ground resolution, the movement trend and geometry and other environmental factors, such as the land-cover type and the topography. Specifically, the presence of vegetation and radar distortion due to surface topography highly limits the reliability of interferometric results. Furthermore, SAR interferometry is not sensitive to north–south movements and thus other techniques should be exploited to retrieve such component of the displacement, e.g. Multiple Aperture InSAR (MAI) (Bechor & Zebker, 2006) and Pixel Offset (OP) (Manconi et al., 2014).

The advanced multi-temporal PS and SBAS interferometric techniques, providing displacement time series of surface slow deformations, are extremely useful in risk mapping to monitor phenomena like subsidence and landslides.

As far as rapid mapping is concerned, the conventional differential interferometric technique (DInSAR) is one of the most adopted approaches thanks to its low processing-time, its low number of input data required and its capacity to delineate the areas affected by large and sudden deformations. DInSAR is also useful to monitor some phenomena such as magma activity and seasonal aquifer changes. Since more recently, coherence information analyses allow scientists to detect changes induced by disasters, e.g. the presence of new lava flows in case of volcano eruptions.

Nevertheless, considering the tight time constraint of rapid mapping activities, interferometric approaches are currently exploited mainly for risk analyses rather than for Rapid Mapping activities. The main factors that limit a wider operational use of interferometry-based information are as follows.

- The availability of suitable SAR acquisitions immediately after the event, since having access to proper interferometric pairs may require several days in the worst case scenario. This is of course one of the main limiting factors, although the increase of future sensors and constellations may mitigate this specific issue, increasing the probability of having proper pre-event data over a specific area of interest.
- The long processing times required by the most advanced techniques is another drawback. Ad hoc hardware setup would be required to significantly reduce the processing time.

The numerous currently available SAR missions provide data characterized by different space resolutions, off-nadir angles and signal frequencies, i.e. the main factors that influence the final results. Therefore, a proper analysis should be carried out to choose the sensor that best fulfills the requirements of a specific application. The availability of comprehensive historical archives dated back to 1992 (ERS-1); hence, it is possible to study past surface behavior, which may be an important feature in risk-related analysis. The decrease of revisiting time of the currently operational missions with respect to the past missions (i.e. week/days revisiting time compared to month revisiting time) strengthens the emergency

mapping capabilities of the interferometric applications; however, it is still not enough to always satisfy the rapid mapping time requirement. Next-generation Terrasar-X missions, due to advanced SAR sensor technology, will lead to spatial resolution up to 0.25 m (TSX-NG 2016). On the other hand, also the second-generation Cosmo-SkyMed mission, composed by two satellites, will be characterized by finer spatial and radiometric resolution and larger coverage (https://directory.eoportal.org/web/eoportal/satellite-missions/c-missions/cosmo-skymed-second-generation).

Disclosure statement

No potential conflict of interest was reported by the authors.

References

Antonietta, F., Boccardo, P., Giulio Tonolo, F., & Vassileva, M. (2015). Damage assessment exploiting remote sensing imagery: Review of the typhoon haiyan case study. *IEEE International Geoscience and Remote Sensing Symposium (IGARSS)*. doi:10.1109/IGARSS.2015.7326589

ARPA Piemonte (2016). Agenzia regionale per la protezione ambientale. *Geoviewer 2D*. Retrieved from http://webgis.arpa.piemonte.it/flxview/GeoViewerArpa/

Bechor, N.B.D., & Zebker, H.A. (2006). Measuring two-dimensional movements using a single InSAR pair. *Geophysical Research Letters*, *33*, L16311. doi:10.1029/2006GL026883

Berardino, P., Fornaro, G., Lanari, R., & Sansosti, E. (2002). A new algorithm for surface deformation monitoring based on small baseline differential SAR interferometry. *IEEE Aerospace and Electronic*, *40*. doi:10.1109/TGRS.2002.803792

Bianchini, S., Ciampalini, A., Raspini, F., Bardi, F., Di Traglia, F., Moretti, S., & Casagli, N. (2015). Multi-temporal evaluation of landslide movements and impacts on buildings in San Fratello (Italy) by means of C-band and X-band PSI data. *Pure and Applied Geophysics (Springer)*, *172*, 3043–3065. doi:10.1007/s00024-014-0839-2

Boccardo, P., Gentile, V., Giulio-Tonolo, F., Grandoni, D., & Vassileva, M. (2015). Multitemporal SAR coherence analysis: Lava flow monitoring case study. *2015 IEEE International Geoscience and Remote Sensing Symposium (IGARSS)*. doi:10.1109/IGARSS.2015.7326370

Boccardo, P., & Giulio-Tonolo, F. (2014). Remote sensing role in emergency mapping for disaster response. *Engineering Geology for Society and Territory*, *5*, 17–24. ISBN: 978-3-319-09047-4. doi: 10.1007/978-3-319-09048-1_3

Casagli, N., Cigna, F., Bianchini, S., Hölbling, D., Füreder, P., Righini, G., … Bianchi, M. (2016). Landslide mapping and monitoring by using radar and optical remote sensing: Examples from the EC-FP7 project SAFER. *Remote Sensing Applications: Society and Environment*, *4*, 92–108. doi:10.1016/j.rsase.2016.07.001

Central Italy earthquakes, 10/2016. (2016). Sentinel interferogram of the 26/10/2016 and 30/10/2016 seismic events in central Italy. Retrieved from http://beyond-eocenter.eu/index.php/geophysical/earthquakes/central-italy-2016

Colesanti, C., Ferretti, A., Prati, C., & Rocca, F. (2003). Monitoring landslides and tectonic motions with the permanent scatterers technique. *Engineering Geology*, *68*, 3–14. doi:10.1016/S0013-7952(02)00195-3

COSMO-SkyMed Second Generation (CSG) Constellation (2016). *eoPortal Directory*. Retrieved from https://directory.eoportal.org/web/eoportal/satellite-missions/c-missions/cosmo-skymed-second-generation

Crosetto, M. (2002). Calibration and validation of SAR interferometry for DEM generation. *ISPRS Journal of Photogrammetry & Remote Sensing*, *57*, 213–227. doi:10.1016/S0924-2716(02)00107-7

EMSR111: Volcanic eruption at Fogo Island (Cape Verde). (2014). Copernicus emergency management service. Retrieved from http://emergency.copernicus.eu/mapping/list-of-components/EMSR111

Ferretti, A., Prati, C., & Rocca, F. (2000). Nonlinear subsidence rate estimation using permanent scatterers in differential SAR interferometry. *IEEE Transactions on Geoscience and Remote Sensing*, *38*, 2202–2212. doi:10.1109/36.868878

Ferretti, A., Prati, C., & Rocca, F. (2001). Permanent scatterers in SAR interferometry. *IEEE Transactions Geoscience Remote Sensing*, *39*, 8–20. doi:10.1109/36.898661

Gabriel, A.K., Goldstein, R.M., & Zebker, H.A. (1989). Mapping small elevation changes over large areas: Differential radar interferometry. *Journal of Geophysical Research*, *94*, 9183–9191. doi:10.1029/JB094iB07p09183

Haghighi, M.H., & Motagh, M. (2016). Assessment of ground surface displacement in Taihape landslide, New Zealand, with C- and X-band SAR interferometry. *New Zealand Journal of Geology and Geophysics*, *59*, 136–146. doi:10.1080/00288306.2015.1127824

Harris, R.A. (1998). Introduction to special section: Stress trigger, stress shadows, and implication for seismic hazard. *Journal of Geophysical Research*, *103*, 24,347–24,358. doi:10.1029/98JB01576

Hooper, A., Zebker, H., Segall, P., & Kampes, B. (2004). A new method for measuring deformation on volcanoes and other natural terrains using InSAR persistent scatterers. *Geophysical Research Letters*, *31*. doi:10.1029/2004GL021737

International Working Group on Satellite-based Emergency Mapping (IWG-SEM) V.A. (2014). Emergency mapping guidelines. Working Paper (v1.0). Retrieved from http://www.un-spider.org/sites/default/files/IWG_SEM_EmergencyMappingGuidelines_A4_v1_March2014.pdf

Jónsson, S., Zebker, H.A., Segall, P., & Amelung, F. (2002). Fault slip distribution of the 1999 Mw7.2 HectorMine earthquake, California, estimated from satellite radar and GPS measurements. *Bulletin Seism Social American*, *92*, 1377–1389. doi:10.1785/0120000922

Lanari, R., Casu, F., Manzo, M., Zeni, G., Berardino, P., Manunta, M., & Pepe, A. (2007). An overview of the small baseline subset algorithm: A DInSAR technique for surface deformation analysis. *Pure and Applied Geophysics*, *164*, 637–661. 0033–4553/07/040637–25. doi: 10.1007/s00024-007-0192-9

Manconi, A., Casu, F., Ardizzone, F., Bonano, M., Cardinali, M., De Luca, C., … Guzzetti, F. (2014). Brief communication: Rapid mapping of landslide events: The 3 December 2013 Montescaglioso landslide, Italy. *Natural Hazards Earth Systems Sciences*, *14*, 1835–1841. doi:10.5194/nhess-14-1835-2014

Marquardt, D. (1963). An algorithm for least-squares estimation of nonlinear parameters. *Journal of the Society for Industrial and Applied Mathematics*, *11*, 431–441. doi:10.1137/0111030

Mason, D.C., Trigg, M., Garcia-Pintado, J., Cloke, H.L., Neal, J.C., & Bates, P.D. (2016). Improving the TanDEM-X Digital Elevation Model for flood modelling using flood extents from synthetic aperture radar images. *Remote Sensing of Environment*, *173*, 15–28. doi:10.1016/j.rse.2015.11.018

Mogi, K. (1958). Relations between eruptions of various volcanoes and the deformation of the ground surface around them. *Bulletin Earth Researcher Institute*, *36*, 99–134.

Perez, F., Cámaro, W., Angeluccetti, I., Demarchi, A., & Boccardo, P. (2015). Analysis of vegetation dynamics and precipitation in Africa for drought monitoring purposes. *Geoscience and Remote Sensing Symposium (IGARSS), 2015 IEEE International*. doi:10.1109/IGARSS.2015.7326234

Piacentini, D., Devoto, S., Mantovani, M., Pasuto, A., Prampolini, M., & Soldati, M. (2015). Landslide susceptibility modeling assisted by Persistent Scatterers Interferometry (PSI): An example from the northwestern coast of Malta. *Nat Hazards*, *78*, 681–697. doi:10.1007/s11069-015-1740-8

Prati, C., Ferretti, A., & Perissin, D. (2010). Recent advances on surface ground deformation measurement by means of repeated space-borne SAR observations. *Journal of Geodynamics*, *49*, 161–170. doi:10.1016/j.jog.2009.10.011

Rosen, P.A., Hensley, S., Joughin, I.R., Li, F.K., Madsen, S. N., Rodrìguez, E., & Goldstein, R.M. (2000). Synthetic aperture radar interferometry. *Proceedings of the IEEE*, *88*, 333–382. doi:10.1109/5.838084

Tofani, V., Raspini, F., Catani, F., & Casagli, N. (2013). Persistent Scatterer Interferometry (PSI) technique for landslide characterization and monitoring. *Remote Sensing*, *5*, 1045–1065. doi:10.3390/rs5031045

TSX-NG (TerraSAR-X Next Generation) (2016). *eoPortal Directory*. Retrieved from https://directory.eoportal.org/web/eoportal/satellite-missions/t/tsx-ng

Vassileva, M., Nascetti, A., GiulioTonolo, F., & Boccardo, P. (2015). Unsupervised flood extent detection from SAR imagery applying shadow filtering from SAR simulated image. *2015 IEEE International Geoscience and Remote Sensing Symposium (IGARSS)*. doi:10.1109/IGARSS.2015.7326372

Voigt, S., Giulio-Tonolo, F., Lyons, J., Kučera, J., Jones, B., Schneiderhan, T., … Guha-Sapir, D. (2016). Global trends in satellite-based emergency mapping. *Science*, *353*, 247–252. doi:10.1126/science.aad8728

Zhang, J.Z., Huang, H., & Bi, H. (2014). Land subsidence in the modern Yellow River Delta based on InSAR time series analysis. *Nat Hazards*, *75*. doi:10.1007/s11069-014-1434-7

Zhu, L., Gong, H., Li, X., Wang, R., Chen, B., Dai, Z., & Teatini, P. (2015). Land subsidence due to groundwater withdrawal in the northern Beijing plain, China. *Engineering Geology*, *193*, 243–255. doi:10.1016/j.enggeo.2015.04.020

Zuo, R., Qu, C., Shan, X., Zhang, G., & Song, X. (2016). Coseismic deformation fields and a fault slip model for the Mw7.8 mainshock and Mw7.3 aftershock of the Gorkha-Nepal 2015 earthquake derived from Sentinel-1A SAR interferometry. *Tectonophysics*, *686*, 158–169. doi:10.1016/j.tecto.2016.07.032